Space Weather

RESEARCH ARTICLE
10.1029/2018SW001874

This article is a companion to Sato et al. (2018) https://doi.org/10.1029/2018SW001873.

Special Section:
Space Weather Events of 4-10 September 2017

# Radiation Dose Nowcast for the Ground Level Enhancement on 10–11 September 2017

**Ryuho Kataoka[1,2], Tatsuhiko Sato[3], Shoko Miyake[4], Daikou Shiota[5,6], and Yûki Kubo[5]**

[1]National Institute of Polar Research, Tachikawa, Japan, [2]SOKENDAI, Midori-cho 10-3, Tachikawa, Japan, [3]Japan Atomic Energy Agency, Tokai, Japan, [4]National Institute of Technology, Ibaraki College, Hitachinaka, Japan, [5]National Institute of Information and Communications Technology, Koganei, Japan, [6]Institute for Space-Earth Environmental Research, Nagoya University, Nagoya, Japan

**Abstract** A ground level enhancement event occurred on 10–11 September 2017, associated with an X8.2 solar flare on the western limb of the Sun. We report the results of our manually conducted nowcast using WArning System for AVIation Exposure to Solar energetic particles. The maximum radiation dose rate at a flight altitude of 12 km was estimated to be approximately 3 μSv/h, which is less than half of the dose rate due to galactic cosmic rays. We also discuss a possible quasi-parallel shock-acceleration mechanism that may have led to the exceptionally soft proton energy spectrum as ground level enhancement events.

**Key Points:**
- The radiation dose during the ground level enhancement on 10–11 September 2017 (GLE 72) was manually nowcasted
- The maximum radiation dose rate of GLE 72 at flight altitude was estimated to be 3 μSv/h
- The exceptionally soft proton energy spectrum at 0.1–10 GeV range during GLE 72 may have been caused by a parallel shock acceleration

**Correspondence to:**
R. Kataoka,
kataoka.ryuho@nipr.ac.jp

**Citation:**
Kataoka, R., Sato, T., Miyake, S., Shiota, D., & Kubo, Y. (2018). Radiation dose nowcast for the ground level enhancement on 10–11 September 2017. *Space Weather*, *16*, 917–923. https://doi.org/10.1029/2018SW001874

Received 30 MAR 2018
Accepted 19 MAY 2018
Accepted article online 25 MAY 2018
Published online 30 JUL 2018



## 1. Introduction

A ground level enhancement (GLE) event occurred at 1630 UT on 10 September 2017, associated with an X8.2 solar flare on the western limb of the Sun. The GLE event was the 72nd since the first detected GLE event, which was observed in 1942 by Forbush (1946). One of the most notable characteristics of this event was that the associated coronal mass ejection (CME) had an extremely high speed of approximately 3,400 km/s, corresponding to almost a one-in-one-hundred-years event (Gopalswamy, 2018).

Predicting intense solar energetic particle (SEP) events such as GLE events is challenging and one of the most important aspects of space weather research (Kataoka et al., 2011). We have recently developed a physics-based framework called WASAVIES (WArning System for AVIation Exposure to Solar energetic particles) to nowcast and forecast the development of a GLE and the corresponding radiation dose, as described in a series of papers (Kataoka et al., 2014; Kubo et al., 2015; Miyake et al., 2017; Sato et al., 2014). The detailed calculation algorithm of the latest version of the automated WASAVIES system and its verification are reported in a companion paper (Sato, Kataoka, et al., 2018, S18 hereafter).

Ground level enhancement 72 offered a surprising opportunity for us to improve our capabilities in nowcasting and forecasting the development of GLEs. We applied the WASAVIES to nowcast and quantitatively estimate the possible radiation dose during the GLE 72 event at flight altitude. The purpose of this paper is to present the basic characteristics of the GLE 72 event obtained from this analysis and to identify possible problems that may be encountered in future operations.

## 2. Calculation Procedures

The basic concept of the calculation procedures used in this study was essentially the same as that of the original WASAVIES framework (Kataoka et al., 2014) and is briefly introduced as follows. First, we prepared simulated data sets of time profiles of proton spectra for arbitrary pitch angles as obtained by solving 1-D focused transport equations, varying the time profiles of the initial proton spectrum as controlled by fast, medium, and slow "IPs" and the power-law spectral index, among other parameters (Kubo et al., 2015). Second, these data sets were combined with an antiproton trace model in the magnetosphere to derive the proton flux at the top of atmosphere anywhere in the world (Miyake et al., 2017). Finally, the fluxes of protons and their secondary particles as well as the associated radiation doses in the atmosphere were calculated from the top-of-atmosphere proton flux using an air shower simulation database developed with the Particle and Heavy Ion Transport code System (Sato, Iwamoto, et al., 2018).

In this study, we applied the latest version of WASAVIES, in which we dynamically search for the best fit values of the injection parameter (IP) and the power-law spectral index $\gamma$ of the injected protons as well as the tilt

angle $\theta_t$ and the normalization factor $N_0$ of the SEP flux. The best fit parameters were determined to minimize the errors with respect to the observed proton fluxes at >100 MeV as measured by the GOES satellites in geosynchronous orbit as well as the observed count rates at 13 selected neutron monitors on the ground. These data were automatically downloaded from the National Oceanic and Atmospheric Administration and Neutron Monitor Database websites at intervals of 5 min for the real-time operation of the automated WASAVIES system. More technical details of the automated WASAVIES system are described in a companion paper (S18).

Among the four free parameters, only the tilt angle $\theta_t$ has been newly added in comparison with the original WASAVIES framework to account for the possibility of a large north-south asymmetry of the dose rate, as was seen in GLE 69 (Matthiä et al., 2009). However, since the introduction of the tilt angle is not important in the particular case of GLE 72, we omit any further explanation of the technical details of the automated WASAVIES system here and leave this description to a separate companion paper (S18).

As shown above, the key components of WASAVIES can be summarized as the physics-based transport model of energetic protons from the Sun to the Earth and the air-shower simulation against to the energetic protons. Major assumptions are power-law distribution of the initially injected protons of 0.1–10 GeV and 1-D stochastic transport along the static Parker spiral. Several input parameters including the spectral index of injected protons are needed to run the transport model, and several output data including the dose rate at flight altitude or neutron counts at ground are obtained from the air-shower simulation.

## 3. Results

Figure 1 shows the count rates measured by several neutron monitors during the GLE 72 event and compares them with our calculated data as obtained from WASAVIES. The fluctuations observed in the calculated lines arise from the discrete selections of the best fit parameters. Nevertheless, reasonable agreement can be seen between our model and the observations. For example, the obtained results are consistent with the fact that the increase in the count rates reached only up to approximately 5% at the South Pole, while a significant signal was almost undetectable at Newark.

Figure 2 shows the proton flux at >100 MeV as measured by the GOES 13 satellite in geosynchronous orbit. Our calculated data obtained by varying the power-law spectral index $\gamma$ from 4.5 to 7.0 are also shown. The other parameters were set to their best fit values. It is found that the best fit values of $\gamma$ during the increasing and decreasing phases of the event are approximately 6.0 and 7.0, respectively, both of which are exceptionally high, as the typical value of the spectral index $\gamma$ is 5.0 (e.g., Duggal, 1979). A higher $\gamma$, that is, a softer proton spectrum, results in a lesser impact at the ground level even when the proton fluxes in geosynchronous orbit are very high, as discussed by Kataoka et al. (2015).

Figure 3 shows the calculated effective dose rates due to SEP exposure at various altitudes. The dose rates due to galactic cosmic rays (GCRs), as calculated with the Particle and Heavy Ion Transport code System-based analytical radiation model PARMA, version 4 (Sato, 2015), are also shown. The highest dose rates among the 432 locations (18 latitudes × 24 longitudes) are plotted in the graph to present the most conservative radiation dose estimates. It is evident that the SEP dose rates were generally lower than the corresponding GCR dose rates during the GLE 72 event, except at the altitude of 20 km. For example, the maximum SEP dose rate at a conventional flight altitude of 12 km was estimated to be approximately 3 μSv/h, which is less than half of the corresponding GCR dose rate.

The total SEP dose delivered to aircrews as estimated under the most conservative scenario, that is, remaining at the highest-dose locations at 12 km for the entire duration of GLE, is approximately 36 μSv, which is only one third of the GCR dose (~0.1 mSv) received during the round trip between Tokyo and New York. It is also confirmed that the SEP dose dramatically increased with increasing altitude in comparison to the GCR dose. The total SEP dose at 20 km for the entire duration of GLE 72 was 0.91 mSv at maximum, which is 25 times higher than the corresponding value at 12 km.

One of the most impressive improvements in the automated WASAVIES system is the real-time display of the spatial distribution of the radiation dose rate across the world. Figure 4 shows an example snapshot of the global map of the SEP radiation dose during GLE 72.

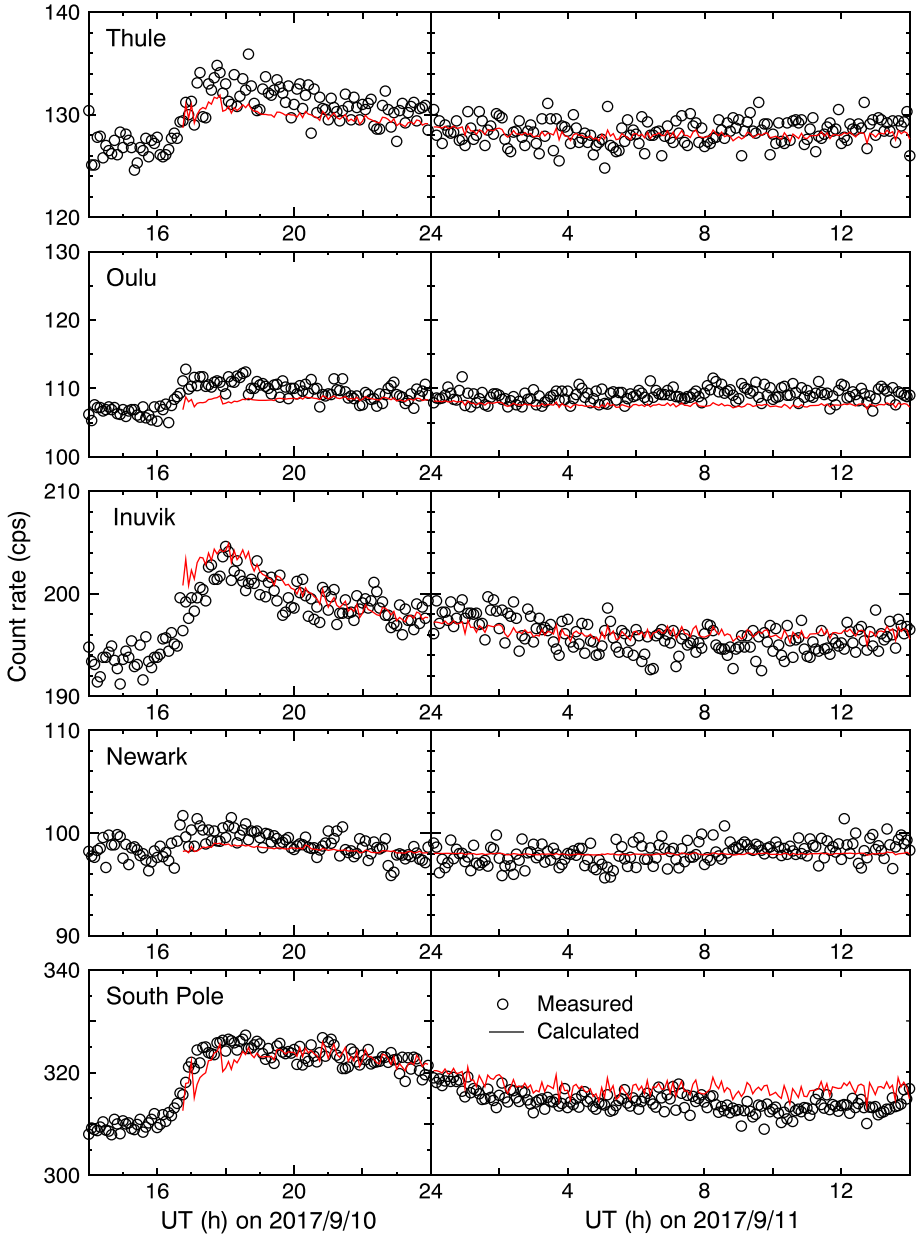


**Figure 1.** Measured count rates (circles) at the neutron monitors at Thule (76.5°N, 68.7°W), Oulu (65.05°N, 25.47°E), Inuvik (68.36°N, 133.72°W), Newark (39.68°N, 75.75°W), and South Pole (90.0°S) during GLE 72, compared against our calculated data (red lines).

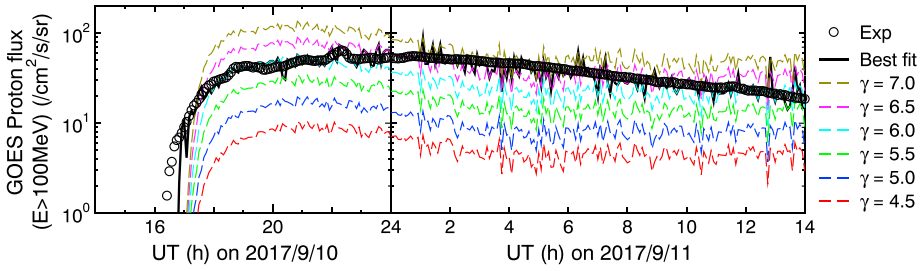


**Figure 2.** Proton flux at >100 MeV as measured by the GOES satellites (circles), compared against our calculated data (dashed curves) obtained by varying the power-law spectral index γ of the injected protons from 4.5 to 7.0.

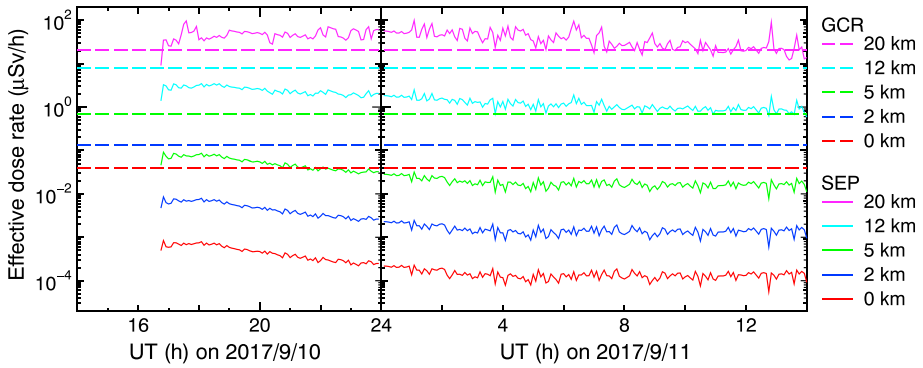


**Figure 3.** Highest effective dose rates among the 432 locations at various altitudes due to solar energetic particle exposure (solid curves) and galactic cosmic ray exposure (dashed lines).

## 4. Discussion

Figure 5 shows that the relatively long-duration time profile of the GLE 72 event can be mostly fitted with slow IP, as expected; this is a typical feature of a limb event, as previously discussed by Kataoka et al. (2014). It is again found from Figure 5 that the value of the spectral index $\gamma$ lies mostly between 6 and 7, which is exceptionally high for GLEs. Based on this result, we conclude that the GLE 72 event is exceptionally soft as GLE events, comparing with many other GLE events (see S18), although it has been reported that the GLE 72 event was one of the hardest SEP events during the weak solar cycle 24 (Schwadron et al., 2018).

To understand the realistic situation in the space environment, it is useful to examine the results from a dynamic three-dimensional magnetohydrodynamic simulation of the inner heliosphere, which includes both realistic background solar wind structures and CMEs. Figure 6 shows the solar wind speed distribution on the ecliptic plane as reproduced by the SUSANOO-CME model (Shiota & Kataoka, 2016), in which multiple magnetized CMEs can be launched. The extremely high-speed CME was launched toward the west, as observed. However, the entire extent of the CME was sufficiently large to be a halo-type CME, as was observed from the Earth (Figure 7), which is roughly consistent with the overall results from the SUSANOO-CME model. It is noteworthy that Schwadron et al. (2018) also obtained similar results of the disturbance in the inner heliosphere using a different CME model.

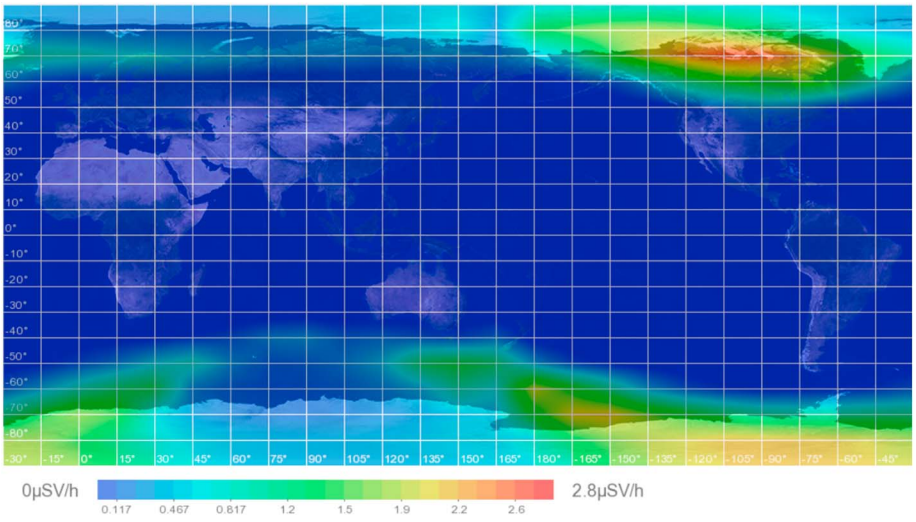


**Figure 4.** Global map of the calculated effective dose rates due to solar energetic particles at a 12-km altitude at 18:00 UT on 10 September 2017.

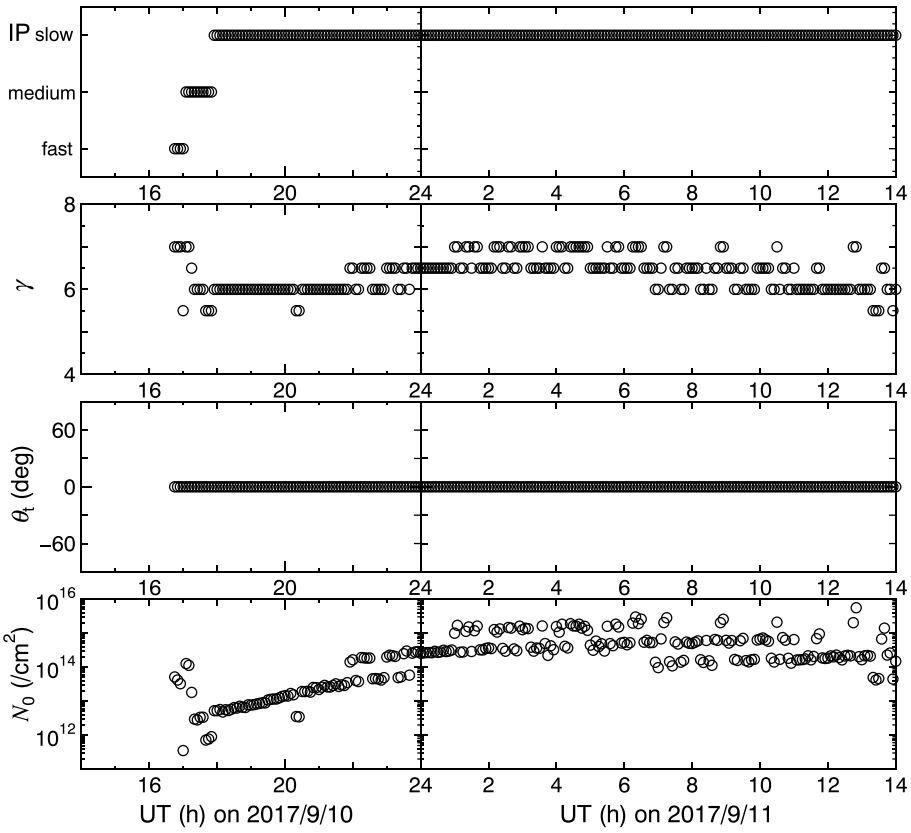


**Figure 5.** Best fit parameters from WArning System for AVIation Exposure to Solar energetic particles for reproducing the observed data from neutron monitors and GOES satellites during the GLE 72 event. (top to bottom) The injection parameter, the power-law spectral index $\gamma$ of the initial protons, the incident tilt angle $\theta_t$, and the normalization factor $N_0$ of the solar energetic particle flux.

Figure 7 shows differential images of the observed halo CME. The deformation of the 360° halo-type structure, especially on the east side of the Sun, is associated with a neutral sheet of slow and dense plasma, in which the speed of the CME is relatively reduced. Such deceleration and deformation of CMEs have been theoretically predicted in other studies (Odstrčil & Pizzo, 1999; Riley et al., 1997). It is also found from the SUSANOO-CME model (Figure 6) that the flank side of the extremely fast CME was deformed against the slow

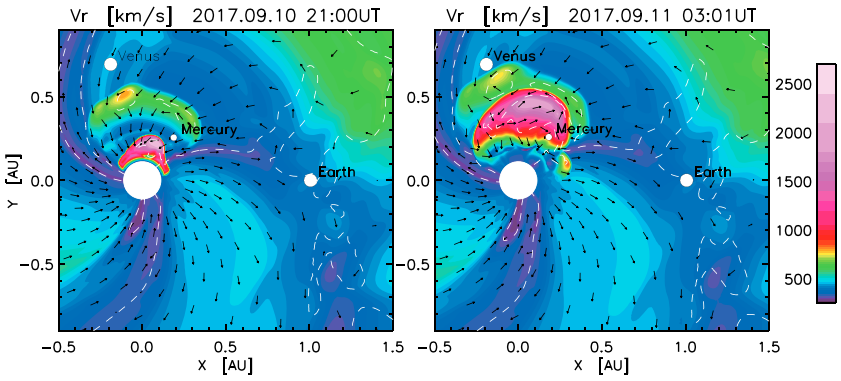


**Figure 6.** The solar wind structures on the ecliptic plane as reproduced by the SUSANOO coronal mass ejection (CME) model. The colors indicate the solar wind speed, and the arrows indicate the directions of the interplanetary magnetic field. Neutral lines are also represented by white dashed curves. During the GLE 72 event, the Earth was predominantly connected to the deformed flank side of the extremely fast CME via a radially aligned interplanetary magnetic field.

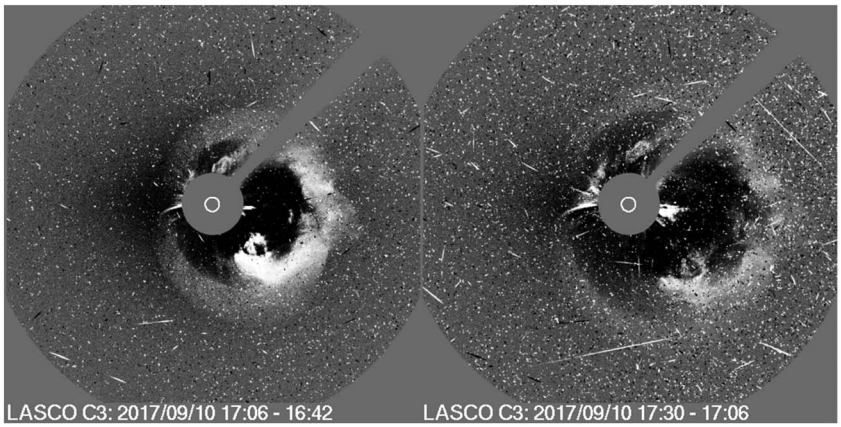


**Figure 7.** Differential images observed by the SOHO/LASCO C3 coronagraph. The time evolution of the rapidly increasing flux of energetic protons can also be recognized from the damage of proton trajectories.

and dense plasma around the neutral line. Furthermore, it is found that preceding CMEs gave rise to a somewhat radially aligned interplanetary magnetic field structure upstream of the Earth. The relatively small-scale shock wave therefore faced more directly toward the Earth, allowing it to accelerate and propagate the SEPs along the approximately radial interplanetary magnetic field.

The reduced speed of the small-scale shock wave was still high (above 1,000 km/s), and the CME-driven shock was likely strong enough to rapidly create GeV particles. In fact, Gopalswamy et al. (2012) showed that all of GLEs during solar cycle 23 had associated CME speed of $>$1,000 km/s. Although the power-law index from standard diffusive acceleration theory (Bell, 1978; Blandford & Ostriker, 1978) depends only on the compression ratio, it is possible that the actual energy spectrum of a shock-accelerated spectrum from 0.1 to 10 GeV range depends on the shock angle, which is defined as the angle between the shock normal and the interplanetary magnetic field. This is because the acceleration of quasi-perpendicular shocks is rapid, giving them a distinct advantage in producing high-energy particles (e.g., Giacalone et al., 1994; Jokipii, 1987; Zank et al., 2004). Also, considering Ellison-Ramaty type (Ellison & Ramaty, 1985) power-law spectra with a exponential cut-off at high energy, the magnetic geometry can have an effect of about one order of magnitude on the cut-off energy (Sandroos & Vainio, 2009). The cut-off energy should also depend on the size of shocks. The small-scale shock wave had a mostly small shock angle; that is, the shock was quasi-parallel during the GLE event, as shown in Figure 6. The exceptionally soft spectrum of GLE 72 can therefore be consistent with the special situation of the deformed CME.

Multiple CMEs arrived at to the Earth before the GLE 72 event, and a major Forbush decrease event occurred before and during GLE 72. The Forbush event was in the recovery stage when the GLE 72 event occurred. The background GCR dose rate was therefore different from the typical rate on quiet days, which can pose a problem for the correct real-time evaluation of the pure contribution due to the GLE. It is therefore important to regularly obtain well-determined background GCR level. In the current WASAVIES system, the average background count rate for 10–85 min before the detection of the GLE is automatically used to fit the increasing count rates of the neutron monitors; consequently, the background count rates that were subtracted to evaluate the increasing count rates during the GLE 72 event were 2–4% smaller than usual due to the Forbush decrease. The question of how to automatically assess the background level in real time during Forbush events will be addressed in future work.

In summary, it is important to obtain an overview and the time-dependent hitory of the solar wind structures in the inner heliosphere with the help of three-dimensional magnetohydrodynamic simulations to understand the possibly complex situations that may lead to unexpected features of GLEs. Nevertheless, it has also been demonstrated in this study that WASAVIES is a useful tool for the space weather nowcasting of GLEs. For example, WASAVIES was capable of quantitatively estimating the SEP radiation dose and identifying the exceptionally soft spectrum of GLE 72 in real time. We believe that this study provides a good example of such bidirectional research-to-operation and operation-to-research development for space weather research and operations.

**Acknowledgments**
We wish to thank Mr. T. Tsujino at Science Graphics Co. Ltd. for developing a program for visualizing the dose rate map calculated by WASAVIES. We acknowledge the Neutron Monitor Database (www.nmdb.eu), funded under the European Union's FP7 Programme (contract 213007), for providing the data. The neutron monitors of the Bartol Research Institute are supported by the National Science Foundation. We thank the Sodankyla Geophysical Observatory of the University of Oulu for providing their neutron monitor data. The coronagraph data were provided by SOHO/LASCO. GOES proton data were provided by National Oceanic and Atmospheric Administration/NGDC. This work was partially supported by JSPS KAKENHI grants (26106006, 15H05813, 15H05815, and 17K05671). The preparation of this paper was supported by an NIPR publication subsidy. The calculated data from WASAVIES and SUSANOO-CME for the GLE 72 event are available upon request.

## References

Bell, A. R. (1978). The acceleration of cosmic rays in shock fronts—I. *Monthly Notices of the Royal Astronomical Society*, *182*(2), 147–156. https://doi.org/10.1093/mnras/182.2.147

Blandford, R. D., & Ostriker, J. P. (1978). Particle acceleration by astrophysical shocks. *Astrophysical Journal. Letters*, *221*, L29.

Duggal, S. P. (1979). Relativistic solar cosmic rays. *Reviews of Geophysics and Space Physics*, *17*(5), 1021.

Ellison, D. C., & Ramaty, R. (1985). Shock acceleration of electrons and ions in solar flares. *Astrophysical Journal*, *298*, 400–408.

Forbush, S. E. (1946). Three unusual cosmic-ray increases possibly due to charged particles from the Sun. *Physical Review*, *70*(9–10), 771–772. https://doi.org/10.1103/PhysRev.70.771

Giacalone, J., Jokipii, J. R., & Kota, J. (1994). Ion injection and acceleration at quasi-perpendicular shocks. *Journal of Geophysical Research*, *99*(A10), 19,351–19,358. https://doi.org/10.1029/94JA01213

Gopalswamy, N. (2018). Extreme solar eruptions and their space weather consequences. In N. Buzulukova (Ed.), *Extreme events in the geospace: Origins, predictability and consequences* (Part 2, pp. 37–63). Elsevier.

Gopalswamy, N., Xie, H., Yashiro, S., Akiyama, S., Makela, P., & Usoskin, I. G. (2012). Properties of ground level enhancement events and the associated solar eruptions during solar cycle 23. *Space Science Reviews*, *171*(1–4), 23–60.

Jokipii, J. R. (1987). Rate of energy gain and maximum energy in diffusive shock acceleration. *Astrophysical Journal*, *313*, 842–846.

Kataoka, R., Nakagawa, Y., & Sato, T. (2015). Radiation dose of aircrews during a solar proton event without ground-level enhancement. *Annales de Geophysique*, *33*(1), 75–78. https://doi.org/10.5194/angeo-33-75-2015

Kataoka, R., Sato, T., Kubo, Y., Shiota, D., Kuwabara, T., Yashiro, S., & Yasuda, H. (2014). Radiation dose forecast of WASAVIES during ground level enhancement. *Space Weather*, *12*, 380–386. https://doi.org/10.1002/2014SW001053

Kataoka, R., Sato, T., & Yasuda, H. (2011). Predicting radiation dose on aircraft from solar energetic particles. *Space Weather*, *9*, S08004. https://doi.org/10.1029/2011SW000699

Kubo, Y., Kataoka, R., & Sato, T. (2015). Interplanetary particle transport simulation for warning system for aviation exposure to solar energetic particles. *Earth, Planets and Space*, *67*(1), 117. https://doi.org/10.1186/s40623-015-0260-9

Matthiä, D., Heber, B., Reitz, G., Meier, M., Sihver, L., Berger, T., & Herbst, K. (2009). Temporal and spatial evolution of the solar energetic particle event on 20 January 2005 and resulting radiation doses in aviation. *Journal of Geophysical Research*, *114*, A08104. https://doi.org/10.1029/2009JA014125

Miyake, S., Kataoka, R., & Sato, T. (2017). Cosmic ray modulation and radiation dose of aircrews during the solar cycle 24/25. *Space Weather*, *15*, 589–605. https://doi.org/10.1002/2016SW001588

Odstrčil, D., & Pizzo, V. J. (1999). Three-dimensional propagation of coronal mass ejections (CMEs) in a structured solar wind flow: 1. CME launched within the streamer belt. *Journal of Geophysical Research*, *104*(A1), 483–492. https://doi.org/10.1029/1998JA900019

Riley, P., Gosling, J. T., & Pizzo, V. J. (1997). A two-dimensional simulation of the radial and latitudinal evolution of a solar wind disturbance driven by a fast, high-pressure coronal mass ejection. *Journal of Geophysical Research*, *102*(A7), 14,677–14,685. https://doi.org/10.1029/97JA01131

Sandroos, A., & Vainio, R. (2009). Diffusive shock acceleration to relativistic energies in the solar corona. *Astronomy and Astrophysics*, *507*(2), L21–L24.

Sato, T. (2015). Analytical model for estimating terrestrial cosmic ray fluxes nearly anytime and anywhere in the world: Extension of PARMA/EXPACS. *PLoS One*, *10*(12), e0144679.

Sato, T., Iwamoto, Y., Hashimoto, S., Ogawa, T., Furuta, T., Abe, S. I., et al. (2018). Features of Particle and Heavy Ion Transport code System PHITS version 3.02. *Journal of Nuclear Science and Technology*, *55*(6), 684–690. https://doi.org/10.1080/00223131.2017.1419890

Sato, T., Kataoka, R., Shiota, D., Kubo, Y., Ishii, M., Yasuda, H., et al. (2018). Real-time and automatic analysis program for WASAVIES: Warning system of aviation exposure to solar energetic particles. *Space Weather*, *16*. https://doi.org/10.1029/2018SW001873

Sato, T., Kataoka, R., Yasuda, H., Seiji, Y., Kuwabara, T., Shiota, D., & Kubo, Y. (2014). Air shower simulation for WASAVIES: Warning system for aviation exposure to solar energetic particles. *Radiation Protection Dosimetry*, *161*(1-4), 274–278.

Schwadron, N. A., Rahmanifard, F., Wilson, J., Jordan, A. P., Spence, H. E., Joyce, C. J., et al. (2018). Update on the worsening particle radiation environment observed by CRaTER and implications for future human deep-space exploration. *Space Weather*, *16*, 289–303. https://doi.org/10.1002/2017SW001803

Shiota, D., & Kataoka, R. (2016). Magnetohydrodynamic simulation of interplanetary propagation of multiple coronal mass ejections with internal magnetic flux rope (SUSANOO-CME). *Space Weather*, *14*, 56–75. https://doi.org/10.1002/2015SW001308

Zank, G. P., Li, G., Florinski, V., Matthaeus, W. H., Webb, G. M., & le Roux, J. A. (2004). Perpendicular diffusion coefficient for charged particles of arbitrary energy. *Journal of Geophysical Research*, *109*, A04107. https://doi.org/10.1029/2003JA010301